

MODELLING THE IMPACT OF TSUNAMIS ON COASTAL DEFENCES IN THE UK

Maurice V. McCabe¹, Peter K. Stansby¹, Lee S. Cunningham¹ and Benedict D. Rogers¹

This paper describes a study that is part of a wider project investigating whether climate change will increase the risk to the UK from tsunamis caused by submarine landslides in the Arctic. Here, the nearshore modelling of tsunamis and damage to coastal structures will be investigated. Therefore a shallow-water and Boussinesq (SWAB) model has been coupled to a mass-spring model to investigate nearshore wave-structure interactions. This coupled model has been tested against experimental data for wall deflection due to solitary waves and caisson sliding due to regular waves. Although some results are promising, further investigation is required before using this technique as a predictive tool.

Keywords: tsunami modelling; nearshore; Boussinesq model; wave forces; wave-structure interaction

INTRODUCTION

In the UK, coastal structures are designed to withstand the combinations of large waves and extreme water levels associated with storms. The widespread damage caused by multiple Atlantic storms over winter 2013 has highlighted our vulnerability, which will be expected to increase with climate change and sea level rise. Tsunamis, on the other hand, appear to be extremely rare in the UK. There is evidence that the south-western coast of England received tsunami waves of up to 3 m in height from the 1755 Lisbon earthquake (Borlase, 1755). Additionally, there have been several recorded tsunami-like occurrences that have been attributed to meteorological events – so-called meteo-tsunamis (Monserrat et al, 2006) – such as the severe flooding of the land around the Bristol Channel in 1607 (Horsburgh and Horritt, 2006). The Storegga submarine landslide occurred off the west coast of Norway approximately 7900 years ago. The slide itself was estimated to be 95,000 km² in area (Haflidason et al, 2004). Tsunami deposits have been found along the east coast of Scotland as well as the Orkney and Shetland Islands; Smith et al. (2004) estimated that maximum tsunami runup levels were approximately 25 m above contemporary mean high water spring tide levels (MHWS) in the Shetland Islands, and 5 m above contemporary MHWS on the Scottish mainland.

Despite the rarity of such events, there is evidence that earthquakes may be caused by postglacial rebound (Arvidsson, 1996). It is also possible that the break-down and release of gas hydrates in marine sediments could cause slope failure similar to the Storegga slide; increasing sea temperatures would make this mechanism more likely. Therefore, although the risk posed by tsunamis to the UK coast may be less than that from storms, it is worthwhile considering their potential impact.

Modelling overview

The aim of this study is to assess present and future submarine-landslide tsunami risk to the UK's coastal infrastructure. Vulnerable locations along the North Sea coasts of Scotland and England have been selected as modelling locations. Tsunamis will be generated and propagated from various locations in the Norwegian Sea using Fluidity, which is a 3D finite element numerical model. Hill et al. (2014) have published results for their Fluidity simulations of the Storegga tsunami, including the present-day bathymetry, as well as an estimated contemporary bathymetry and sea level. Fig.1 shows a Fluidity simulation of the Storegga tsunami propagating southwards along the east coast of Scotland, using a present day bathymetry.

The Fluidity model, as used by Hill et al. (2014), does not simulate a moving shoreline, so outputs will be generated at various locations in the North Sea. These will form inputs to the Shallow Water and Boussinesq (SWAB) model to be used in the nearshore. The SWAB model has been coupled with a damped mass-spring model, to enable movements of breakwaters and other coastal structures to be estimated.

In this paper, the SWAB model and its coupling to the mass-spring model will be described. Initial results for forces on walls and associated displacements will be presented in comparison to data from physical model tests. This is followed by an application of the mass-spring model to a moving caisson case comparing with experimental data.

¹ School of Mechanical, Civil and Aerospace Engineering, University of Manchester, Manchester, M13 9PL, UK

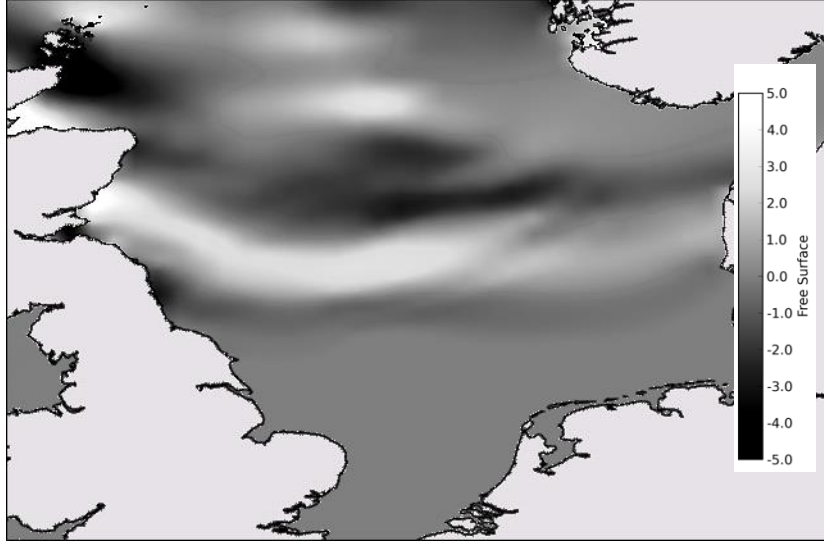


Figure 1. Fluidity simulation of Storegga tsunami propagation in North Sea, with present-day bathymetry, from Hill (2014).

THE SWAB MODEL

Model equations and solver

The SWAB model is described in detail by McCabe et al. (2013). It is based on the widely tested equations of Madsen and Sørensen (1992). They consist of a continuity equation (Eq. 1) and a momentum equation (Eq. 2), given in one dimension as:

$$\frac{\partial h}{\partial t} + \frac{\partial(hu)}{\partial x} = 0 \quad (1)$$

$$\begin{aligned} \frac{\partial(hu)}{\partial t} + \frac{\partial(hu^2)}{\partial x} = & -gh \frac{\partial h}{\partial x} - gh \frac{\partial z_b}{\partial x} - \frac{\tau_b}{\rho} \\ & + \left\{ \left(B + \frac{1}{3} \right) d^2 \left(\frac{\partial^3(hu)}{\partial x^2 \partial t} \right) + Bgd^3 \frac{\partial^3 \eta}{\partial x^3} \right. \\ & \left. + d \frac{\partial d}{\partial x} \left(\frac{1}{3} \frac{\partial^2(hu)}{\partial x \partial t} + 2Bgd \frac{\partial^2 \eta}{\partial x^2} \right) \right\}_{\text{non-breaking}} \\ & + \left\{ \frac{\partial}{\partial x} \left(h \nu_e \frac{\partial u}{\partial x} \right) \right\}_{\text{breaking}} - F_{\text{wall}} = 0 \end{aligned} \quad (2)$$

where $h(x,t)$ is water depth; $u(x,t)$ is depth-averaged horizontal velocity; $\eta(x,t)$ is the free-surface level above an arbitrary datum; $z_b(x)$ is the bed level; $d(x)$ is still water depth; $\tau_b(x,t)$ is bed shear stress; and ν_e is the wave breaking eddy viscosity. B is a constant that controls the linear dispersion characteristics, with a value of 1/15. The model equations were derived assuming small bed slopes and are therefore not suited to the modelling of steep revetments and vertical walls without modification: F_{wall} takes account of this, being derived from the force imposed on a jet of water in a breaking wave impacting against a wall. McCabe et al. (2013) showed that inclusion of this reverse momentum term could greatly improve predictions of volumes for waves overtopping a revetment with a recurve wall, although McCabe et al. (2014) showed that it contributes little to the total force imposed on a wall by a breaking wave. McCabe et al. (2013) give further detail on the equations, the finite volume solver and the method used for calculating wave breaking.

Mass-spring model

For analysis of structural movements due to wave impact, the SWAB model has been coupled to a damped mass-spring model. This is a one-way coupling: hydrodynamic forces feed into the mass-spring model, but structural deflections do not affect the hydrodynamics. The mass-spring part of the SWAB model solves the equation:

$$\mathbf{M}\ddot{\mathbf{x}} + \mathbf{C}\dot{\mathbf{x}} + \mathbf{K}\mathbf{x} = \mathbf{F}(t) \tag{3}$$

where \mathbf{x} is the vector of the movement of the mass, with the number of components of \mathbf{x} being the number of degrees of freedom of the system; the dot notation represents differentiation with respect to time. Because all the cases described here are in one horizontal dimension, \mathbf{x} will have either one (horizontal displacement, x) or two degrees of freedom (horizontal displacement, x , and rotation in x,z plane, θ). \mathbf{M} , \mathbf{C} and \mathbf{K} are matrices of mass/moment of inertia, damping and spring constants respectively. $\mathbf{F}(t)$ is the vector of applied forces and moments. Eq. 3 is calculated at each time-step. For a one-degree-of-freedom system, the following equations are solved in order:

$$\dot{x}^{n+1} = \dot{x}^n + \ddot{x}^n \Delta t \tag{4}$$

$$x^{n+1} = x^n + \dot{x}^{n+1} \Delta t \tag{5}$$

$$\ddot{x}^{n+1} = \frac{F(t) - c_x \dot{x}^{n+1} - k_x x^{n+1}}{m} \tag{6}$$

where m represents mass; c represents a damping coefficient; and k represents a spring constant. These equations give values for position, velocity and acceleration of the structure at time step $n+1$. This one degree-of-freedom system was tested using the wall deflection dataset of Linton et al. (2013), described below.

The mass-spring model is also set up to simulate the caisson sliding case of Wang et al. (2006). In this scenario, a caisson breakwater is able to rotate and slide (if static friction is overcome) over an elastic foundation (Fig. 2).

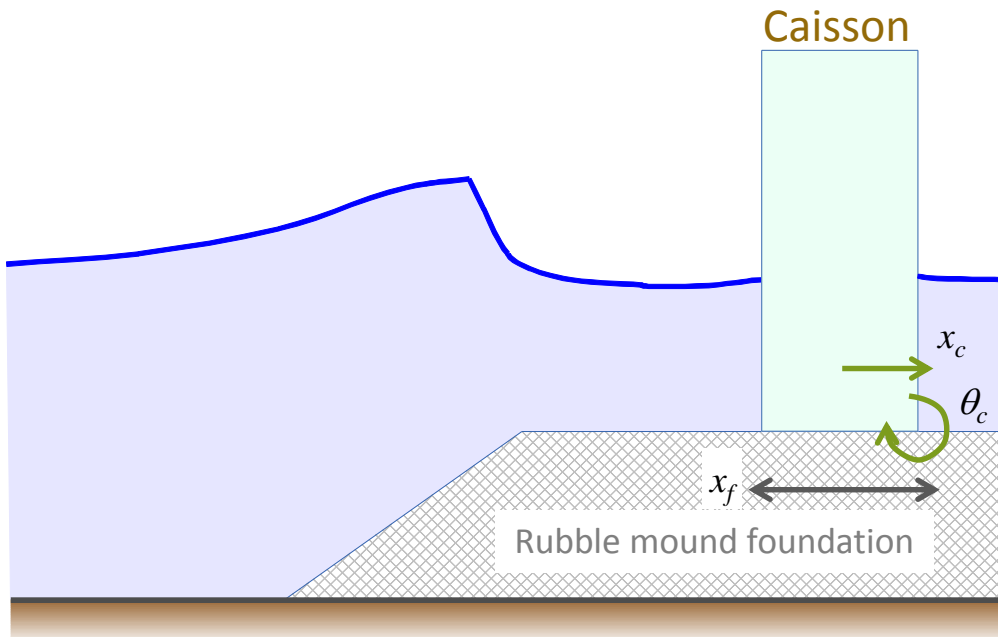


Figure 2. Schematic diagram of caisson and foundation movement of experiments of Wang et al. (2006).

Here, sliding occurs if:

$$F_h > \mu_{st} R \tag{7}$$

where F_h is the horizontal force imposed on the caisson; μ_{st} is the static friction coefficient; and R is the vertical reaction force, which includes the hydrostatic buoyancy force as well as any dynamic forces acting vertically on the caisson. For the non-sliding case, the caisson and foundation move together:

$$\dot{x}_c = \dot{x}_f \quad (8)$$

where the subscripts c and f represent the caisson and foundation respectively. The caisson is able to rotate independently of the foundation, which cannot rotate. \mathbf{M} , \mathbf{C} and \mathbf{K} become:

$$\begin{aligned} \mathbf{M} &= \begin{pmatrix} m_c + m_f & h_g m_c \\ h_g m_c & J + h_g^2 m_c \end{pmatrix} \\ \mathbf{C} &= \begin{pmatrix} c_x & 0 \\ 0 & c_\theta \end{pmatrix} \\ \mathbf{K} &= \begin{pmatrix} k_x & 0 \\ 0 & k_\theta \end{pmatrix} \end{aligned} \quad (9)$$

where J is the moment of inertia of the caisson; and h_g is the vertical distance between the centre of gravity of the caisson and its axis of rotation. Insertion of the values from Eq. 9 into Eq. 2 give two equations, which can both be rearranged in terms of $\ddot{\theta}$. The resulting single equation gives the acceleration of the caisson and foundation, and is equivalent to Eq. 6:

$$\begin{aligned} \ddot{x}_c = \ddot{x}_f &= \frac{(F - c_x \dot{x}_f - k_x x_f)(J + h_g^2 m_c) - (T - c_\theta \dot{\theta} - k_\theta \theta)h_g m_c}{(m_c + m_f)(J + h_g^2 m_c) - (h_g m_c)^2} \\ \ddot{\theta} &= \frac{T - h_g m_c \ddot{x}_c - c_\theta \dot{\theta} - k_\theta \theta}{J + h_g^2 m_c} \end{aligned} \quad (10)$$

where T represents the torque applied to the caisson.

For the sliding case, the caisson moves separately over the foundation. In this case Eq. 8 no longer applies. The only horizontal force between the caisson and elastic foundation is the friction force, F_{fr} . Therefore:

$$\begin{aligned} \ddot{x}_c &= \frac{(F + F_{fr})(J + h_g^2 m_c) - (T - c_\theta \dot{\theta} - k_\theta \theta)h_g m_c}{m_c(J + h_g^2 m_c) - (h_g m_c)^2} \\ \ddot{x}_f &= \frac{-F_{fr} - c_x \dot{x}_f - k_x x_f}{m_f} \end{aligned} \quad (11)$$

with the rotational acceleration being the same as that in Eq. 10. The friction force, F_{fr} , is assumed to be proportional to the normal force between the caisson and the foundation, and acting in the direction opposing motion.

Because the SWAB model is depth averaged it does not give information on vertical velocities in the flow. This presents difficulties when trying to estimate vertical forces. Therefore, the hydrostatic pressure assumption was made: the uplift force acting on the caisson is a function of the instantaneous water depths on either side. Horizontal forces are also assumed to be a function of the instantaneous water depth, plus the force due to the reverse momentum term, which was shown by McCabe et al. (2014) to be relatively small. These forces are shown in Fig. 3.

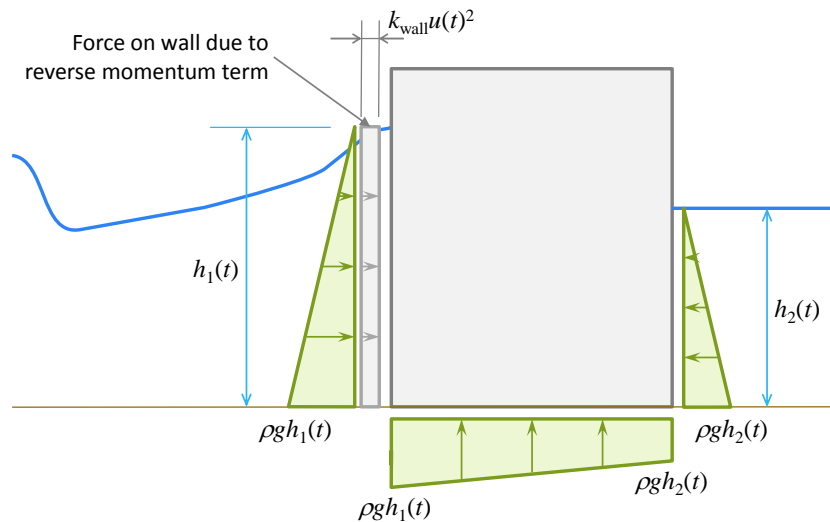


Figure 3. Assumed forces acting on a caisson for mass-spring calculations. k_{wall} is an empirical constant for the reverse momentum term ($k_{wall} = 1$ was used in this study); u is the depth averaged horizontal water velocity at the wall.

SOLITARY WAVES IMPOSED ON A VERTICAL WALL

Experiment description and SWAB implementation

Linton et al. (2013) presented experiments on the tsunami induced loading on wooden vertical walls, above the still water level. The experiments were carried out in the Large Wave Flume at the Network for Earthquake Engineering (NEES) Tsunami Facility at Oregon State University. These experiments used solitary waves to represent the incident tsunami. It should be noted that Madsen et al. (2008) (and others) dispute the use of solitary waves to represent tsunamis, stating that both in the deep ocean and on the continental shelf, the length scale is insufficient for solitary waves to develop. Despite this, the use of repeatable solitary waves is a worthwhile test case and convenient.

The flume layout is shown in Fig. 4. Solitary waves were propagated over 28.6 m of flat bed, with a still water depth of 2.29 m. They then travel over a sloping bed (bed slope, $\cot(\beta) = 10.76$) onto a berm, 0.07 m above the still water level. The vertical walls were positioned 7.3 m from the start of the berm. For this study, two types of wall have been tested; both are vertical stud walls with a 40.6 cm (centre-to-centre) stud spacing, covered with a 13 mm five-ply structural-I plywood. The studs for wall TW1 (Fig. 5) have a 38 mm x 140 mm cross-section, while the studs for wall TW2 have a 38 mm x 88 mm cross-section; these are No.2 (or better) grade kiln-dried Douglas Fir, as defined by the ANSI/AWC NDS-2012 National Design Specification (NDS) for Wood Construction (American Wood Council, 2012). Both walls are supported at the location of the four load cells, which measure horizontal forces. There are also two linear variable differential transformers (LVDTs), placed at the top and bottom of the wall along the centre-line of the flume, used to measure wall deflection.

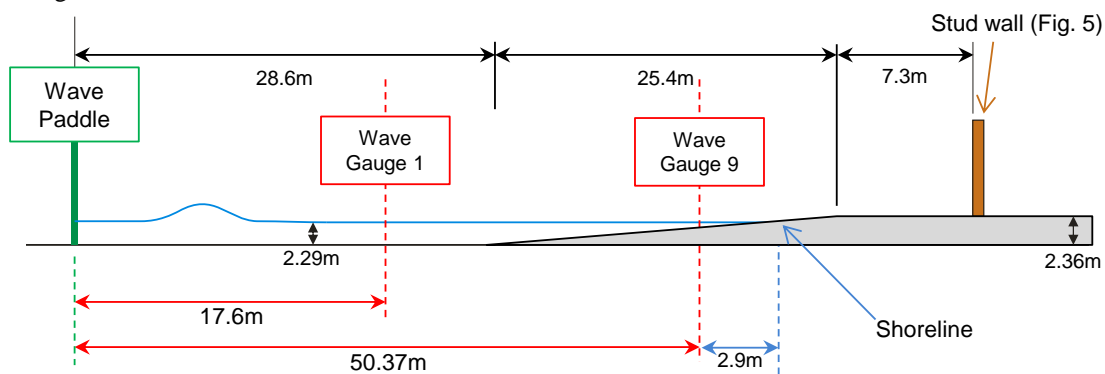


Figure 4. Linton et al. (2013) experimental set-up.

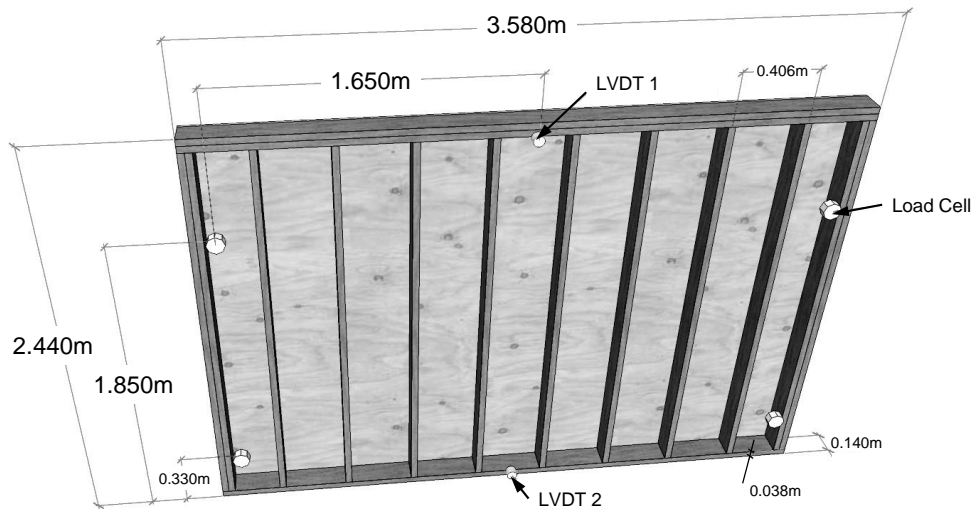


Figure 5. Wall TW1 for Linton et al. (2013) tests.

Values for the dry density, ρ , and Young's modulus, E , of the materials were not given by Linton et al. (2013) so representative values were taken from appropriate manufacturers (Table 1). Note that Young's modulus will decrease and density will increase with moisture content. A kiln-dried wood should have a moisture content of less than 19% (Western Lumber Product Use Manual); however actual moisture contents for the experiments may well have been higher due to the nature of the conditions. This may result in actual values for ρ being higher and E being lower than those adopted below.

Material	Property	Range of values	Value used	Source
No.2 grade Douglas Fir	ρ (kg/m ³)	460 – 500	500	Western Lumber Product Use Manual
12.5mm 5-ply plywood	ρ (kg/m ³)	400 – 600	460	Design Fundamentals (CanPly, 2012)
No.2 grade Douglas Fir	E (GPa)	8.2 – 11.0	8.8	Western Lumber Product Use Manual
12.5mm 5-ply plywood	E (GPa)	7.5 – 11.1	8.8	CanPly Engineered Values

Because a relationship between a static load (at the base of the wall) and the deflection of the stud wall cannot be calculated analytically, a linear static analysis was carried out using the OASYS GSA software suite. The static model applied a uniformly distributed load of 1 kN/m² from the base of the structure to 0.488 m above the base, giving values for deflection across the wall. Maximum deflections, as expected, occur near LVDT 2; values for the spring constant, k_x , used in the SWAB model were based on the ratio between static force and deflection at this location (Table 2). A damping ratio (c_x/c_{cr}) of 0.02 was assumed, though a value of 0.20 had little effect on the results. The critical damping coefficient, c_{cr} was assumed to be:

$$c_{cr} = 2\sqrt{k_x m} \quad (12)$$

Wall	Mass per width, m (kg/m)	OASYS model max. deflection at LDVT 2 (mm)	Spring constant, k_x (kN/m ²)	Critical damping coefficient, c_{cr} (kg/s/m)
TW1	43.3	2	244	6500
TW2	32.6	7	69.7	3020

Results

The SWAB and experiment time-series have been synchronized by setting the time origin $t = 0$ s when the solitary wave crest passes the first wave gauge, on the flat bed 17.6 m from the wave paddle and 43.7 m away from the sea wall. Fig. 6 shows SWAB and experiment time-series at wave gauges 1 and 9, which is the closest to the shoreline, 10.93 m from the wall. The SWAB model gives a good simulation of the main solitary wave, both in terms of magnitude and arrival time.

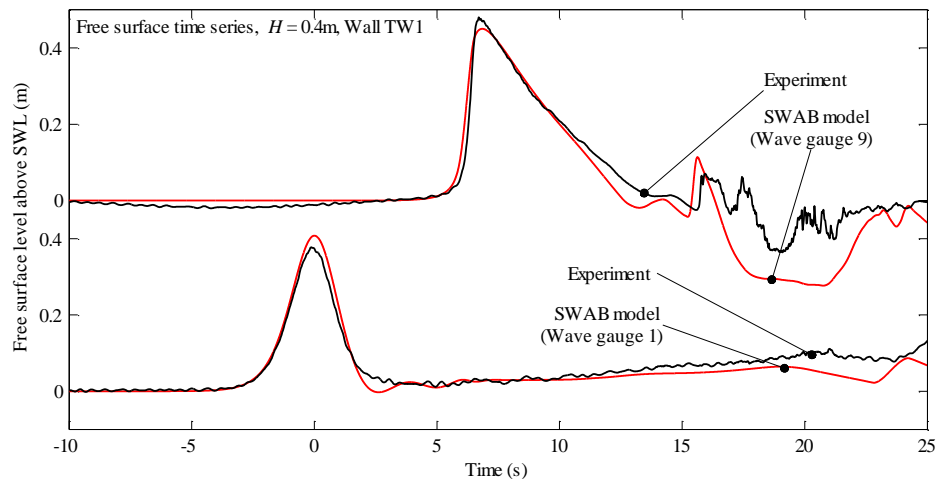


Figure 6. Free surface time series (SWAB and experiment) of solitary wave near wave paddle (wave gauge 1) and near shoreline (wave gauge 9).

Fig. 7 shows time series of loads imposed on both walls. Note that SWAB model predicts the wave to arrive too soon. This requires further investigation; it may be that the SWAB model does not transfer to the nonlinear shallow water equations soon enough, over-predicting the wave speed. This may also cause the bore to be too large, and hence too fast-moving; however at wave gauge 9, the wave in the experiment is slightly larger than the SWAB simulation, suggesting that this is not the case. Nevertheless, the magnitude and duration of the loading predicted by SWAB is reasonable; it does not however give the exact peaks and oscillations in the time-series, which may be because the mass-spring model provides no feedback to the hydrodynamic model.

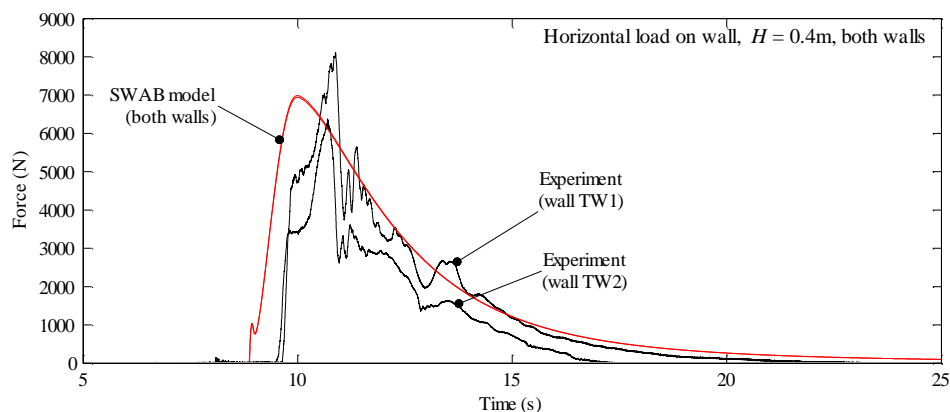


Figure 7. Total horizontal load time series on walls TW1 and TW2 for Linton et al. (2013) experiment and SWAB simulation.

Figs. 8 and 9 show that deflections are of the right order of magnitude, for both walls. For wall TW1, it under-predicts the wall deflection. However, it must be stressed that actual values for the spring constants, could be lower than those estimated due to moisture content. Also, the experiments showed that wall TW2 did not return to its original position; the SWAB model does not take account of any such plastic deformation. The high frequency oscillations shown by the SWAB simulation in Fig. 9 would be related to a damping coefficient that is too low.

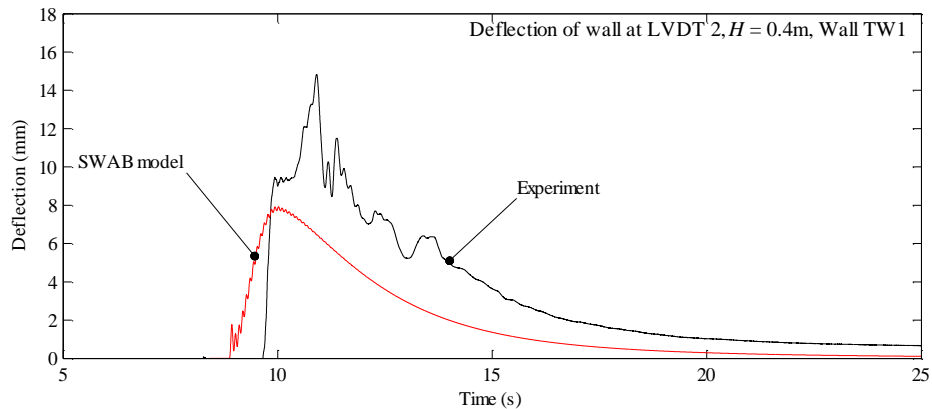


Figure 8. Time series of deflection of wall TW1 at location of LVDT 2 for Linton et al. (2013) experiment and SWAB simulation.

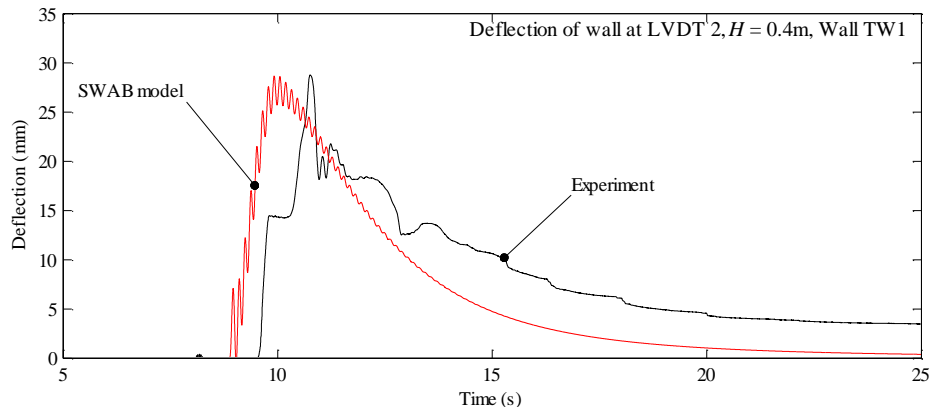


Figure 9. Time series of deflection of wall TW2 at location of LVDT 2 for Linton et al. (2013) experiment and SWAB simulation.

CAISSON OSCILLATION AND SLIDING DUE TO REGULAR WAVE IMPACT

Experiment description and SWAB implementation

Wang et al. (2006) performed experimental tests for the sliding of a caisson due to the impact of breaking regular waves. This case has also been modelled using smoothed particle hydrodynamics (SPH) by Rogers et al. (2010), who predict reasonable agreement for the wave forces and caisson movement. However, in comparison to the SWAB model used here, the SPH simulations are computationally expensive, requiring up to 24 hours to run a simulation. Regular waves were propagated across a 6 m long horizontal bed, with a still water depth of 0.325 m. The waves then travel onto a rubble mound foundation with a slope, $\cot(\beta) = 3$. The caisson is placed 0.2 m from the edge of the crest of the foundation, in a still water depth of 0.15 m. The wave height at the paddle is 0.167 m and the period is 1.3 s; these conditions cause the waves to break on the rubble mound foundation.

The wave conditions at the paddle are nonlinear. The wave form was calculated using the method of Rienecker and Fenton (1981), and converted into a SWAB input using the method described by McCabe et al. (2013). However, the generation of such waves in the SWAB model is problematic; Fig. 10 shows how free components cause water levels and wave heights to vary across the domain.

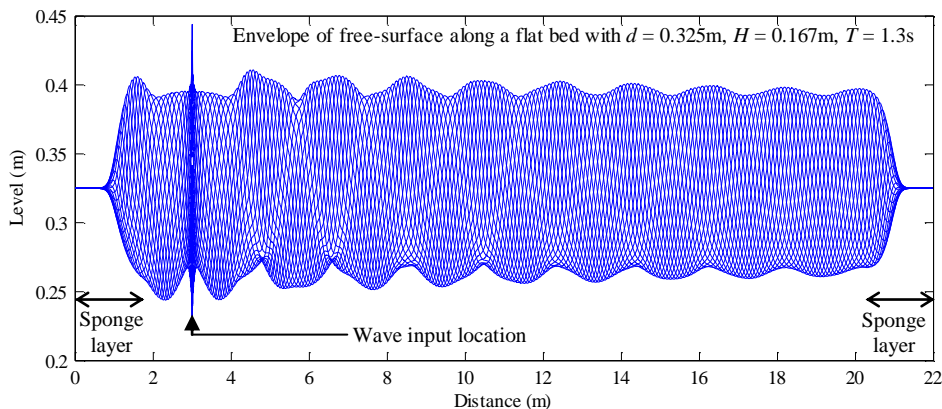


Figure 10. Envelope of free surface levels for SWAB simulation on a horizontal bed, with wave parameters from Wang et al. (2006) experiments.

The caisson is able to vibrate slide over its foundation, and is also able to rotate. The foundation itself is assumed to behave elastically. Values for the mass, spring constants and friction coefficient were taken from the experimental analysis of Wang et al. (2006). In this analysis, damping ratios (c/c_{cr}) were 1.5 times those given by Wang et al. (2006); sensitivity to this parameter will be investigated in future research. The translational critical damping coefficient was calculated using Eq. (12), and the rotational critical damping coefficient was calculated using:

$$c_{cr,\theta} = 2\sqrt{k_{\theta}(J + h_g^2 m)} \quad (13)$$

where the mass m is assumed to be the sum of the mass of the caisson and the hydrodynamic mass moved by the caisson. Although experimental values for this additional mass were given by Wang et al. (2006), based on their natural frequency analysis, these values will not always be available for predictive simulations, so the empirical formulae, given by Cuomo et al. (2011), were used for the numerical scheme. The force acting on the rear of the caisson was assumed to be hydrostatic; this was applied as a constant force in the mass-spring model.

Results

Despite the problems with wave nonlinearity, Fig. 11 shows that both horizontal and vertical forces at the caisson are reasonably well predicted. However, both for the experiment and the SWAB model, there is considerable wave by wave variation; this is not unlikely where waves are breaking close to a vertical structure. It should be noted that the loading period from the SWAB model does not match the experiment; in fact, periods given by the SWAB model were quite variable (between 1.20 s and 1.40 s over 12 waves). It is quite possible that the experiments gave a similar variability; hence the two time-series can quickly move out of phase, as shown in Fig. 11.

The SWAB model shows considerable variation in its simulation of caisson displacement (Fig. 12). For some waves, the caisson sliding distance is similar in magnitude to the experiments, whereas for others the movement is considerably larger. Note the variability of the force imposed by the incident waves, and the very short time over which the horizontal force exceeds the static friction force (Fig. 11). Because the displacement is effectively related to the double integral of this excess force it is not unexpected that some displacements are not well predicted by the SWAB model. Also, the assumptions made in calculating the uplift force will increase the inaccuracy of the SWAB predictions.

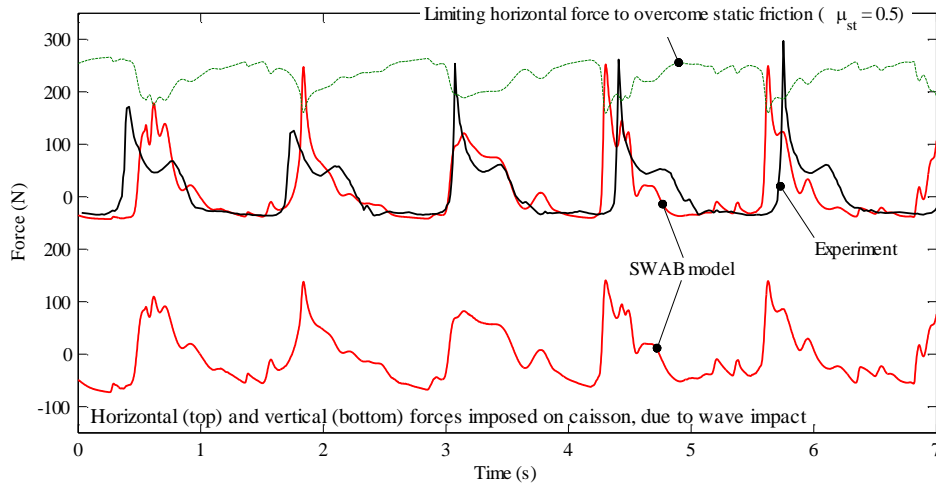


Figure 11. Horizontal and vertical forces acting on caisson, due to wave impact (i.e. force in excess of still-water hydrostatic load). SWAB model simulation of Wang et al. (2006) experiments. Also shown is the limiting horizontal force required for caisson sliding to occur, based on uplift force (Eq. 7). Time origin is arbitrary.

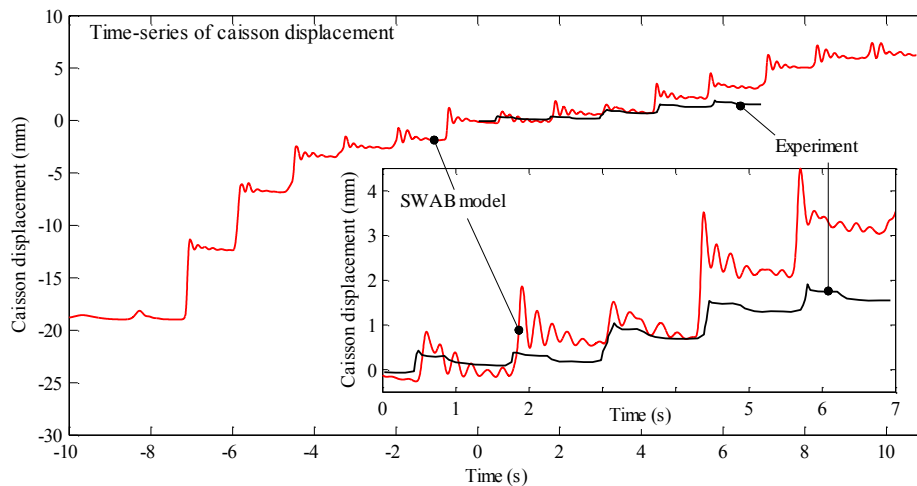


Figure 12. Caisson movement: SWAB simulation alongside Wang et al. (2006) experiments. Time origin is same as that shown in Fig. 11.

CONCLUSIONS

This paper describes our current research on submarine-landslide tsunami risk to the UK, and some of our methodology for investigating how such a tsunami would cause damage to the UK's coastal infrastructure. The shallow water and Boussinesq (SWAB) model, which has previously been shown to predict wave-by-wave overtopping for storm events (McCabe et al. 2013) and wave forces for storm waves and solitary waves (McCabe et al. 2014), has been coupled with a mass-spring model to enable it to calculate movements of coastal structures. SWAB simulations for elastic deflection of a wooden stud wall subject to breaking solitary waves give very promising results, especially considering the uncertainty in the material properties. However, the SWAB model appears to perform less well for calculating oscillation, rotation and sliding of a caisson. There are many sources of error: the nonlinear incident waves; the flow through the porous foundations and highly simplified uplift forces; the short times over which sliding suddenly occurs; and uncertainty and sensitivity to a number of coefficients. Despite this, the coupled model is quick to run and worthy of further testing.

The SWAB model has been developed into a web application (Hu et al, 2013). This provides a user-friendly interface for model pre- and post-processing (Fig. 13). In addition it eliminates the need for any software installation, and can therefore be used on any personal computer, tablet or mobile phone that is connected to the internet. It does not currently include the mass-spring model. This web

application will allow the SWAB model to gain wider use as a tool for research students and coastal engineers. It is available to use at <http://modelling.mace.manchester.ac.uk>; please contact the authors for further information.

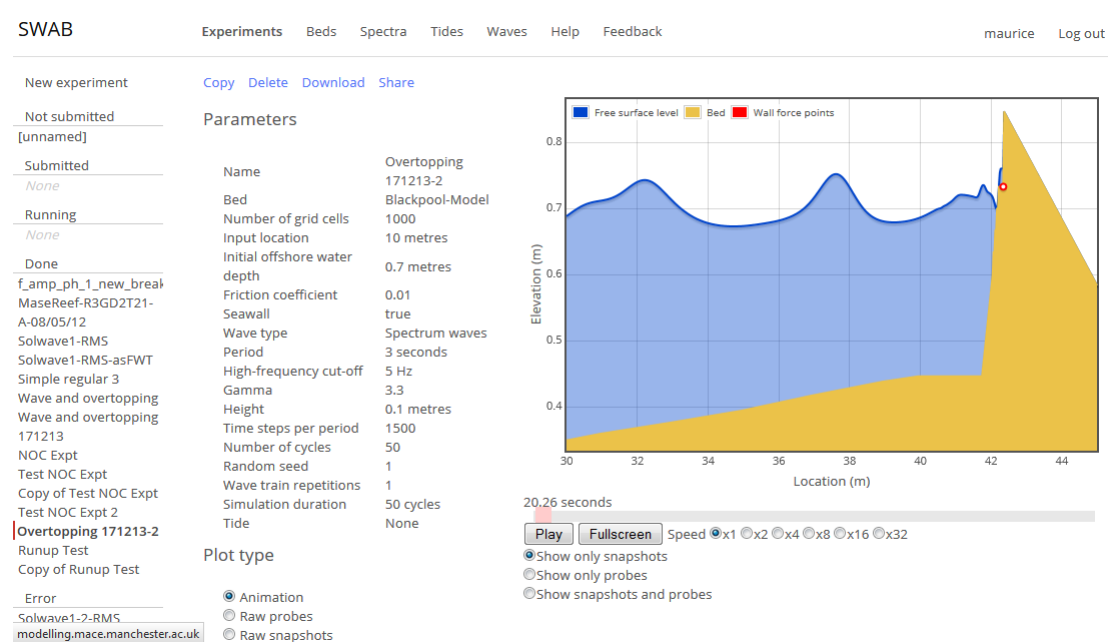


Figure 13. Screenshot of SWAB web application.

ACKNOWLEDGMENTS

This work was supported by the Natural Environment Research Council grant number NE/K000160/1, which is part of the project entitled “Will climate change in the Arctic increase the landslide-tsunami risk to the UK?”, involving teams from the University of Aberdeen, British Geological Survey, University of Cambridge, University of Dundee, Imperial College London, University of Manchester, National Oceanography Centre, University of Southampton and University of Ulster.

The authors would like to thank Dr Jon Hill for supplying the original version of Fig. 1. The authors would also like to thank the Network for Earthquake Engineering Tsunami Research Facility at Oregon State University for making their data publicly available on the web. This is a highly valuable resource.

REFERENCES

- American Wood Council. 2012. *National Design Specification (NDS) for Wood Construction, ANSI/AWC NDS-2012*. American Wood Council, Washington, DC.
- Arvidsson, R. 1996. Fennoscandian earthquakes: whole crustal rupturing related to postglacial rebound, *Science*, 274, 744–746.
- Borlase, W. 1755. Letter to Rev. Charles Lyttleton, *Philosophical Transactions*, 49, 373–378.
- Canadian Plywood Association. 2012. *Plywood Design Fundamentals*, http://www.canply.org/pdf/main/plywood_designfund.pdf, 20 pp.
- Canadian Plywood Association. *CanPly Engineered Values*, <http://www.canply.org/pdf/main/engineered%20values.pdf>, 6 pp.
- Cuomo, G., G. Lupoi, K. Shimosako and S. Takahashi. 2011. Dynamic response and sliding distance of composite breakwaters under breaking and non-breaking wave attack, *Coastal Engineering*, 58, 953–969.
- Haflidason, H., H.P. Sejrup, A. Nygård, J. Mienert, P. Bryn, R. Lien, C.F. Forsberg, K. Berg and D. Masson. 2004. The Storegga Slide: architecture, geometry and slide development, *Marine Geology*, 213, 201–234.

- Hill, J., G.S. Collins, A. Avdis, S.C. Kramer and M.D. Piggott. 2014. How does multiscale modelling and inclusion of realistic palaeobathymetry affect numerical simulation of the Storegga Slide tsunami? *Ocean Modelling*, 83, 11–25.
- Hill, J. 2014. *Personal Communication*.
- Horsburgh, K. and M. Horritt. 2006. The Bristol Channel floods of 1607 – reconstruction and analysis, *Weather*, 61, 272–277.
- Hu, W., M. McCabe, D. Apsley and P. Stansby. 2013. Web application in 1-D shallow water near shore wave simulation, *Journal of Teaching and Education*, 2(2), 509–522.
- Linton, D., R. Gupta, D. Cox, J. van de Lindt, M.E. Oshnack and M. Clauson. 2013. Evaluation of Tsunami Loads on Wood-Frame Walls at Full Scale, *Journal of Structural Engineering*, 139(8), 1318–1325.
- Madsen, P.A., D.R. Fuhrman and H.A. Schäffer. 2008. On the solitary wave paradigm for tsunamis, *Journal of Geophysical Research*, 113, C12012.
- Madsen, P.A. and O.R. Sørensen. 1992. A new form of the Boussinesq equations with improved linear dispersion characteristics. Part 2. A slowly varying bathymetry, *Coastal Engineering*, 18, 183–204.
- McCabe M.V., P.K. Stansby and D.D. Apsley. 2013. Random wave runup and overtopping a steep sea wall: Shallow-water and Boussinesq modelling with generalised breaking and wall impact algorithms validated against laboratory and field measurements, *Coastal Engineering*, 74, 33–49.
- McCabe, M.V., P.K. Stansby, B.D. Rogers and L.S. Cunningham. 2014. Boussinesq modelling of tsunami and storm wave impact, *Proceedings of the ICE – Engineering and Computational Mechanics*, 167(EM3), 106–116.
- Monserrat, S., I. Vilibić and A.B. Rabinovich. 2006. Meteotsunamis: atmospherically induced destructive ocean waves in the tsunami frequency band, *Natural Hazards and Earth System Science*, 6, 1035–1051.
- Rienecker, M.M. and J.D. Fenton. 1981. A Fourier approximation method for steady water waves, *Journal of Fluid Mechanics*, 104, 119–137.
- Rogers, B.D., R.A. Dalrymple and P.K. Stansby. 2010. Simulation of caisson breakwater movement using 2-D SPH, *Journal of Hydraulic Research*, 48, 135–141.
- Smith, D., S. Shi, R.A. Cullingford, A.G. Dawson, S. Dawson, C.R. Firth, I.D.L. Foster, P.T. Fretwell, B.A. Haggart, L.K. Holloway and D. Long. 2004. The Holocene Storegga Slide tsunami in the United Kingdom, *Quaternary Science Reviews*, 23, 2291–2321.
- Wang Y.-Z., Chen, N.-N. and Chi, L.-H. 2005. Numerical simulation on joint motion process of various modes of caisson breakwater under wave excitation, *Communications in Numerical Methods in Engineering*, 22, 535–545.
- Western Wood Products Association. *Western Lumber Product Use Manual*. <http://wwpastore.org/products/western-lumber-products-use-manual>, 24 pp.